

IMU Noise and Performance Characterization

Lab 3 Report

EECE5554: Robotics Sensing and Navigation

Group 4:

Wondmgezahu Teshome (me)

Kanishk Kaushal

Matthew Kazan

Sam Milhaven

March 21, 2025

1 Introduction

The Inertial Measurement Unit (IMU) is a critical component in modern robotic systems, providing essential information about orientation, acceleration, and rotational rates. This lab focuses on the VectorNav VN-100 that combines accelerometers, gyroscopes, and magnetometers to deliver accurate spatial orientation data. Understanding sensor noise characteristics is vital for implementing effective filtering strategies and assessing a sensor's suitability for specific robotic applications. This lab explores various noise sources affecting IMU performance and utilizes Allan variance analysis to characterize key performance parameters including angle random walk, bias stability, and rate random walk.

2 Data Collection

For this experiment, we utilized the VectorNav VN-100 IMU configured to output data at 40 Hz through a custom ROS2 driver. The driver parsed the VNYMR string output from the sensor to extract acceleration, angular velocity, orientation (Euler angles), and magnetometer readings. The data collection was conducted in two distinct environments within the EXP building:

Stationary Data Collection: A 5-minute dataset was recorded on the 2nd floor with the IMU placed on a stable surface.

Dynamic Motion Data Collection: A 5-minute dataset was recorded on the 1st floor, providing space for movement. During this collection, one team member carried the IMU through various motion patterns including walking in straight lines and executing turns, while another team member recorded video of the movements for correlation analysis. For the Allan variance calculation, the dataset was provided in piazza, and we assigned a letter for each team members. In this lab, I used Location B .

3 Results and Analysis

3.1 Stationary Data Analysis

Plots: The following plots show the analysis results for the stationary data.

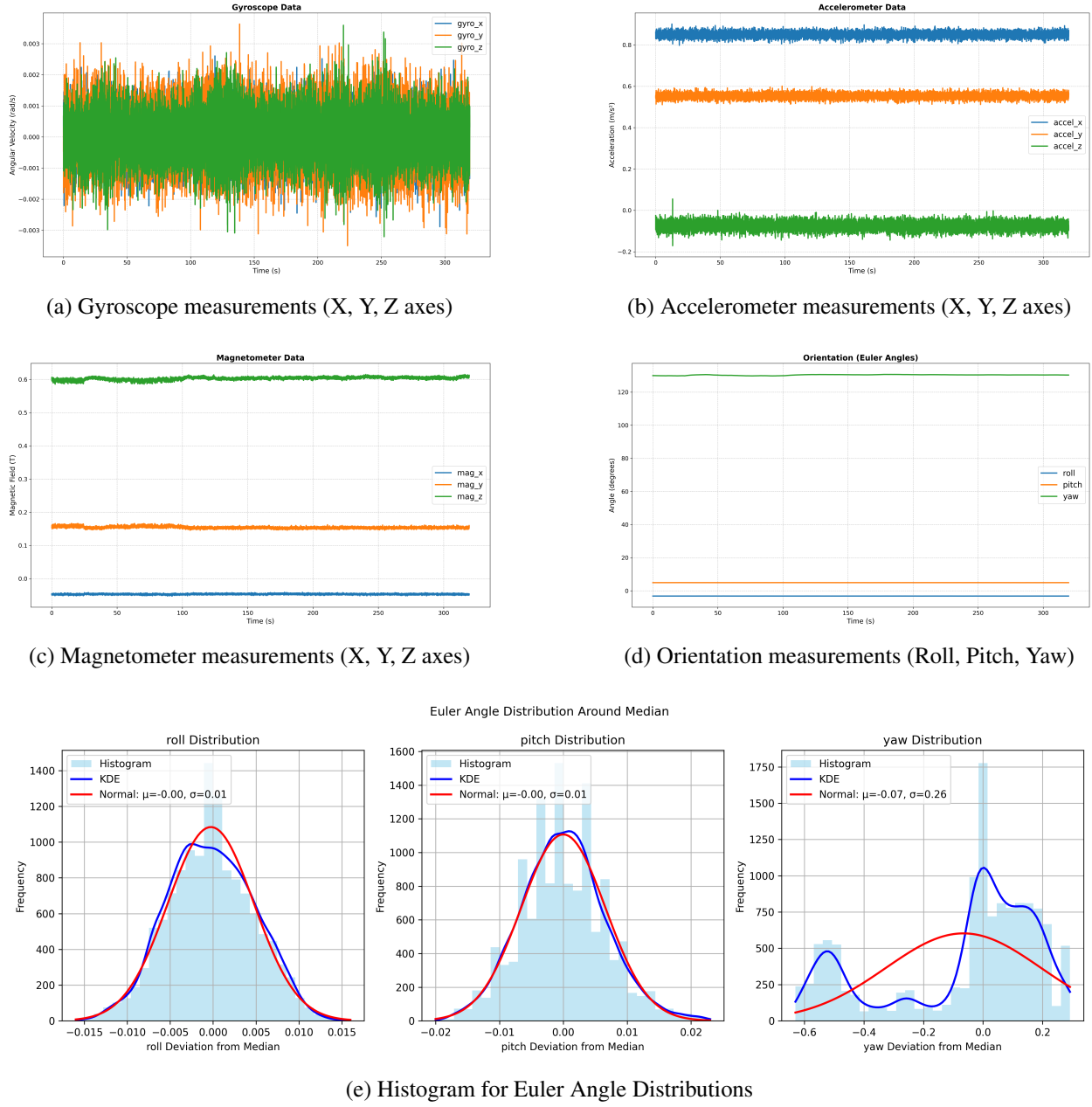


Figure 1: Time series plots of VectorNav VN-100 IMU data collected under stationary conditions (40 Hz sampling rate).

Discussion:

From the above results for the stationary data, we can conclude the following: The VectorNav VN-100 IMU demonstrates stability in orientation measurements over the 300-second collection period. The calculated mean Euler angles (roll: -3.202° , pitch: 4.909° , yaw: 130.358°) closely match the median values (roll: -3.202° , pitch: 4.910° , yaw: 130.424°), indicating minimal bias and drift. This stability is visualized in the orientation time series plot (figure d), which shows nearly flat lines for all three angles. The accelerometer data exhibits small, rapid fluctuations characteristic of white noise, while maintaining consistent mean values on all three axes. Similarly, the magnetometer readings show remarkable stability with minimal fluctuations throughout the measurement period. The gyroscope data oscillates around 0 rad/s for all three axes, with noise amplitude of approximately ± 0.003 rad/s.

Analysis of the **histograms** shows that roll and pitch deviations follow approximately normal distributions with mean 0.00° and standard deviation $\approx 0.01^\circ$. In contrast, the yaw distribution is non-Gaussian with multiple peaks (mean $\approx -0.07^\circ$, standard deviation $\approx 0.26^\circ$). This multimodal distribution in yaw measurements suggests different noise characteristics affecting this axis, likely due to magnetic field variations in the test environment.

Question 1: The stationary data shows low noise levels across all sensors. The accelerometer and gyroscope display typical white noise characteristics with small, rapid, and random fluctuations around their mean values. The magnetometer shows stability with minimal fluctuations. The orientation angles demonstrate a good stability over time, with roll and pitch showing normal distributions of noise, while yaw exhibits a more complex, multimodal noise distribution.

Question 2: As noted above, the mean and median values are very close to each other for all Euler angles, indicating symmetrical distributions for roll and pitch. The distributions for roll and pitch follow approximately normal distributions with small standard deviations ($\sigma \approx 0.01^\circ$), suggesting excellent precision. The yaw angle, however, shows a multimodal distribution with higher variance ($\sigma \approx 0.26^\circ$), which could be due to magnetic interference or sensor fusion algorithm characteristics when calculating yaw, which is common for magnetometer-dependent measurements in indoor environments with magnetic disturbances.

Question 3: For the stationary dataset, a comparison with the VN-100 datasheet specifications shows considerable performance differences. The gyroscope noise levels show fluctuations of approximately ± 0.003 rad/s ($\pm 0.172^\circ/\text{s}$), which is roughly 60 times higher than the specified bias stability of $< 10^\circ/\text{hr} \approx 0.0028^\circ/\text{s}$. Similarly, accelerometer measurements demonstrate fluctuations of approximately $\pm 0.03 \text{ m/s}^2$ ($\pm 3 \text{ mg}$), approximately 75 times higher than the datasheet specification of $< 0.04 \text{ mg}$ ($\approx 0.0004 \text{ m/s}^2$).

Question 4: The significant performance differences between the measured data and datasheet specifications can be primarily attributed to the testing environment on the EXP building's second floor with active student movement. Floor vibrations transmitted through the building structure as students walked would directly impact the readings. The building's structural responses to students moving would introduce low-frequency vibrations detectable by the sensitive IMU. These real-world disturbances contrast sharply with the controlled, vibration-isolated environment typically used for datasheet specifications, explaining the 60-75 \times higher noise levels observed in the measurements.

3.2 Dynamic Motion Analysis

Plots: The following plots show the analysis results for the dynamic motion data under three different clips. The left side shows the timeseries plots, while the right side shows the actual video clips at different timestamps of the recorded motion data.

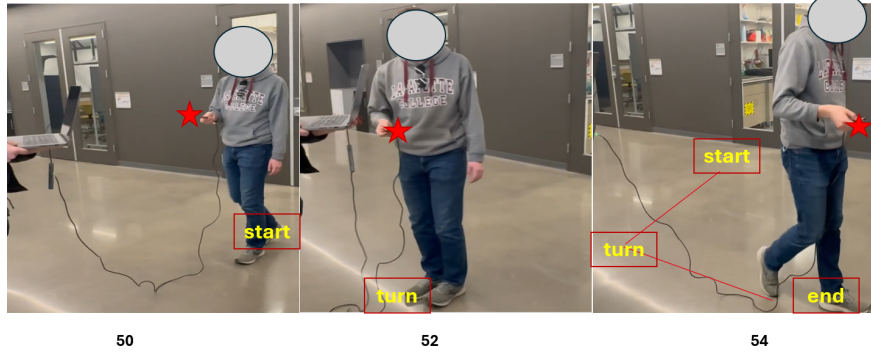


Figure 2: First clip showing timeseries plot (top) and corresponding video clip (bottom) between 50-55 seconds

Observation:

The above IMU data demonstrates correlation with the observed movement in the video clip. The defining feature—the person's left turn at approximately 52 seconds—is clearly captured across all sensor modalities. The gyroscope data shows a pronounced negative spike in the Z-axis (approximately -5 rad/s), which perfectly corresponds to the turning motion shown in the video. The orientation data provides the clearest evidence of the turn, with the yaw angle shifting approximately from $+70^\circ$ to -40° , representing the $\approx 110^\circ$ change in direction. The accelerometer and magnetometer data further confirm this movement pattern, with disruptions in their regular patterns coinciding precisely with the turning action.

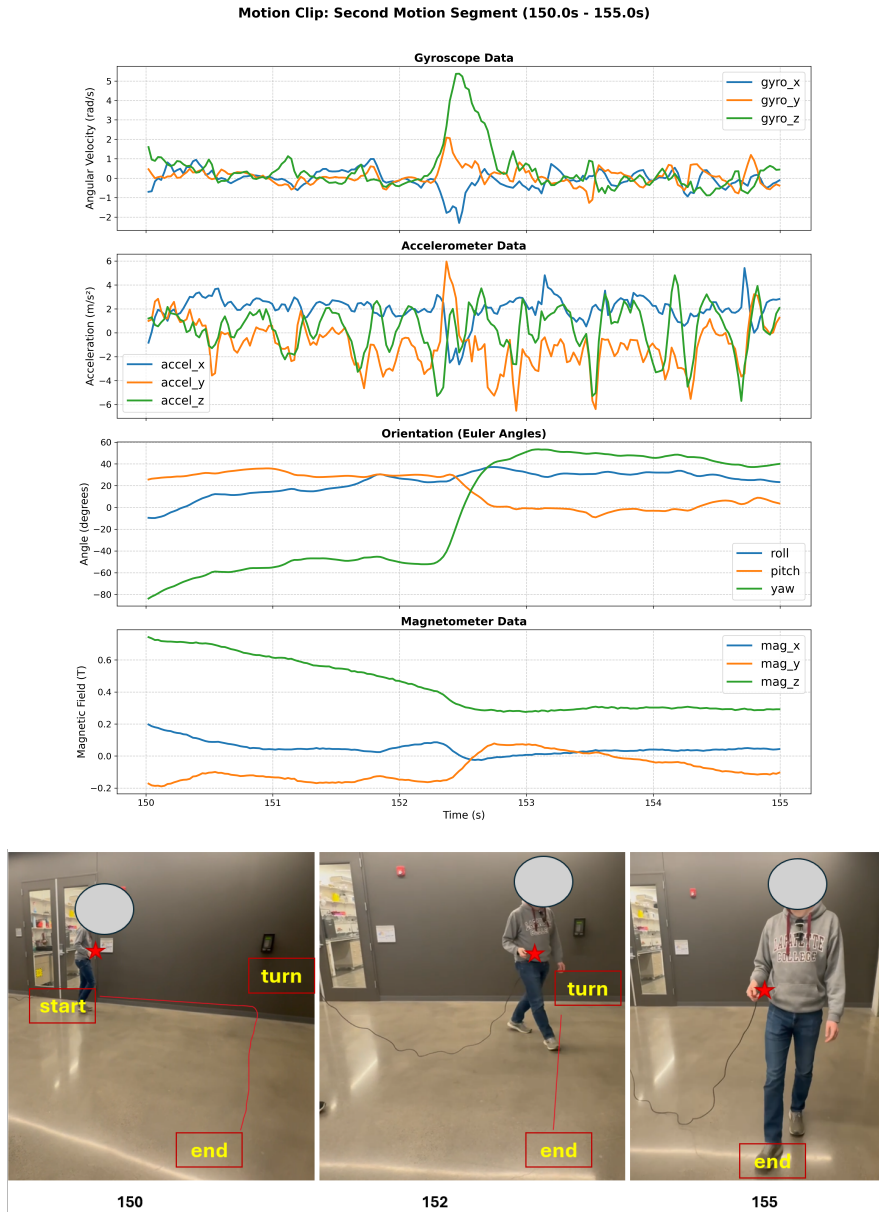


Figure 3: Second clip showing timeseries plot (top) and corresponding video clip (bottom) between 150-155 seconds

Observation: In the second motion clip, the IMU captured a clear right turn at the 152-second mark. The gyroscope data shows a distinctive positive spike (+5 rad/s) in the Z-axis during the turn, correctly indicating clockwise rotation according to the VN-100's right-handed coordinate system. The Euler angles displayed a significant yaw transition from -50° to $+50^\circ$, representing the $\approx 100^\circ$ directional change. Accelerometer readings showed characteristic walking patterns before and after the turn, with notable spikes during the turning maneuver itself. The magnetometer data reinforced these observations, with gradual changes in all three axes that corresponded to the reorientation of the sensor relative to Earth's magnetic field.

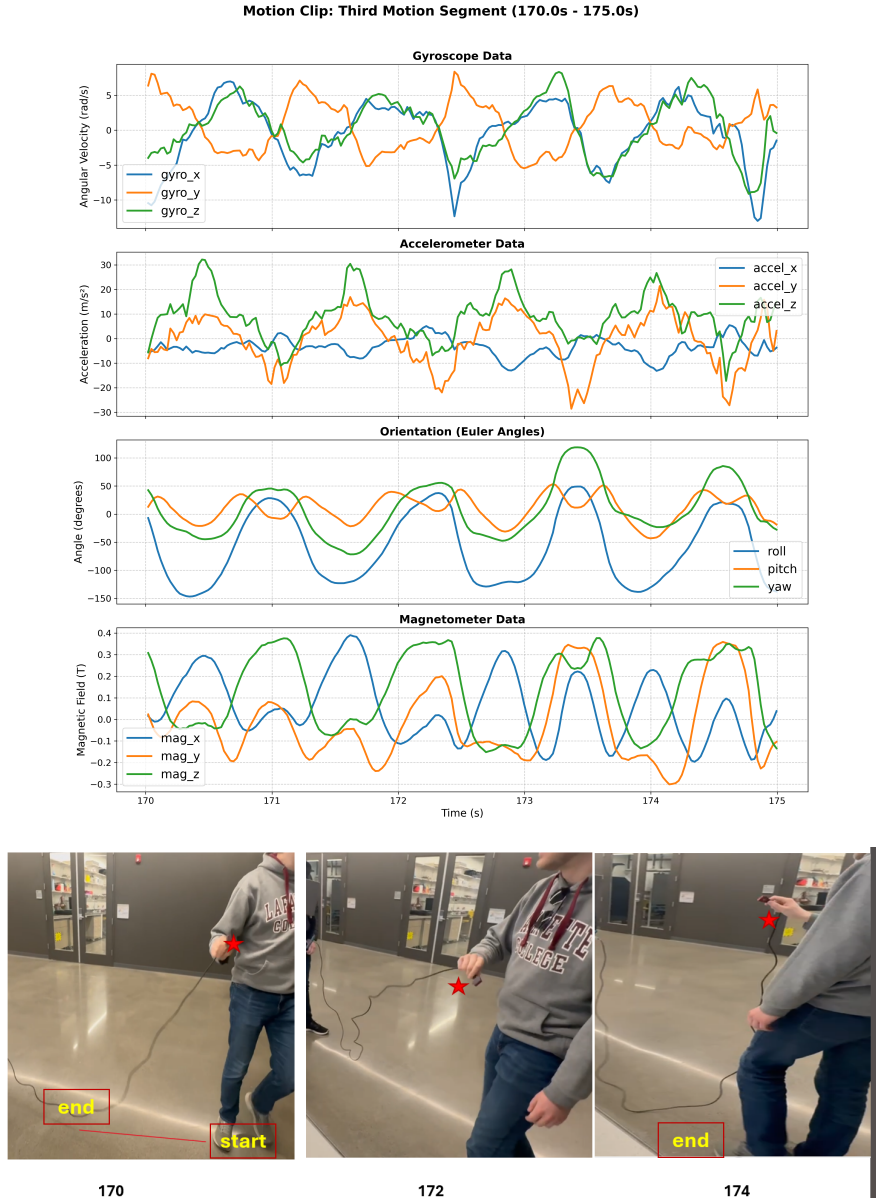


Figure 4: Third clip showing timeseries plot (top) and corresponding video clip (bottom) between 170-175 seconds

Observation: The gyroscope readings show oscillations in all three axes, with angular velocities reaching (-10 to 5 rad/s) far exceeding the values seen in normal walking or turning. These rapid alternating patterns directly correspond to the deliberate flipping motions visible in the video at the 172s and 174s timestamps. The accelerometer data shows another changes, with readings reaching $\pm 30 \text{ m/s}^2$, reflecting the rapid acceleration and deceleration of the device during manipulation. The orientation data shows complete cyclical patterns rather than simple transitions. The roll angle oscillates between 0° and -150° multiple times, while pitch and yaw undergo coordinated periodic changes—clearly demonstrating the full rotation of the device.

Discussion For the motion data, the above figures show 5-second clips for different parts of the video. We collected data for 5 minutes, but the figures highlight selected clips representing key motion patterns. The first clip (50-55s) captured a distinct left turn, with clear corresponding changes in all sensor readings. The second clip (150-155s) demonstrated a right turn with opposing gyroscope and orientation patterns compared to the left turn. The third clip (170-175s) showed complex device manipulation while walking in a straight line, resulting in dramatic oscillations across all sensor modalities.

Question 5: To align the video and VectorNav data, we used a synchronized timestamp approach. First, we started the rosbag recording and video capture simultaneously using a verbal countdown. Then, we performed several distinct motions (like sharp turns and device flips) that would create clear, identifiable patterns in the sensor data. After data collection, these distinctive motion events visible in the video are matched with corresponding spikes or transitions in the sensor data plots.

Question 6: The IMU data demonstrated a correlation with the video footage across all three analyzed segments. In the first clip, the left turn at 52 seconds produced a clear negative spike in gyro_z and a corresponding shift in yaw angle from positive to negative values. The second clip showed the opposite pattern for a right turn, with a positive gyro_z spike and yaw shifting from negative to positive. Notably, the third clip captured the complex device manipulation with dramatic oscillations in all sensor readings that perfectly matched the flipping motions visible in the video. The accelerometer and magnetometer data further supported these correlations.

3.3 Allan Variance Analysis

Plots: The following shows the plot for the allan variance parameters for Location B.

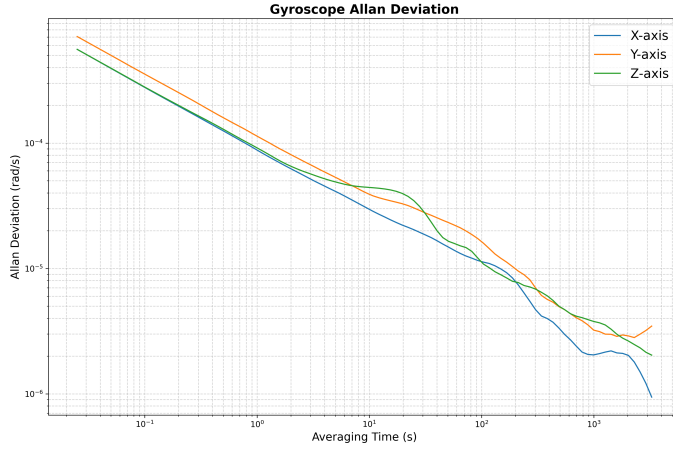


Figure 5: Allan deviation for the Gyroscope data in X, Y and Z axis

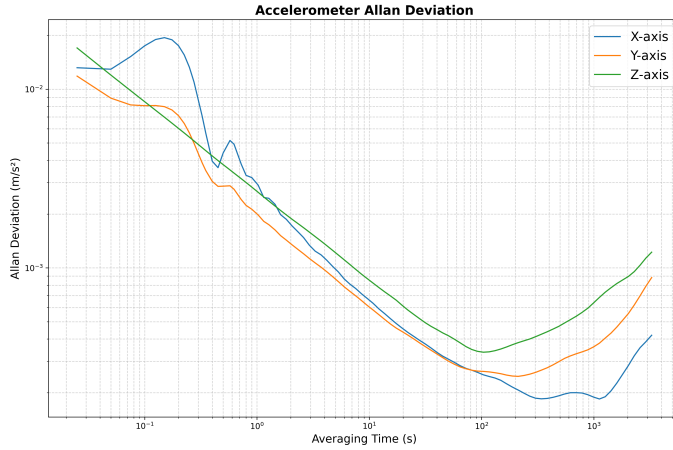


Figure 6: Allan deviation for the Accelerometer data in X, Y and Z axis

Table 1: IMU Noise Parameters for Location B

Parameter	X-axis	Y-axis	Z-axis
Gyroscope			
Angle Random Walk (rad/ \sqrt{s})	8.78×10^{-5}	1.14×10^{-4}	9.12×10^{-5}
Rate Random Walk (rad/s/ \sqrt{s})	1.08×10^{-7}	1.02×10^{-7}	2.48×10^{-5}
Bias Stability (rad/s)	3.10×10^{-6}	4.50×10^{-6}	6.68×10^{-5}
Accelerometer			
Velocity Random Walk (m/s/ \sqrt{s})	2.09×10^{-3}	1.95×10^{-3}	2.72×10^{-3}
Acceleration Random Walk (m/s ² / \sqrt{s})	9.62×10^{-2}	1.97×10^{-5}	3.56×10^{-5}
Bias Stability (m/s ²)	3.01×10^{-4}	1.22×10^{-2}	5.08×10^{-4}

Discussion: The Z-axis gyroscope shows significantly higher Rate Random Walk (2.48×10^{-5} rad/s/ \sqrt{s}) and Bias Stability (6.68×10^{-5} rad/s) compared to X and Y axes, suggesting vertical disturbances. The X-axis accelerometer shows extremely high Acceleration Random Walk (9.62×10^{-2} m/s²/ \sqrt{s}), approximately 1000

times higher than other axes. The accelerometer Allan deviation plot shows distinct irregularities, particularly in the X-axis at short averaging times (0.1-0.5s). The Y-axis has exceptionally high bias stability ($1.22\text{e-}2\text{m/s}^2$), suggesting potential mechanical influence. The irregular patterns in the X-axis accelerometer readings likely indicate proximity to mechanical equipment (HVAC systems, pumps, or elevators) common in building basements. The discontinuities in the curves suggest periodic vibrations from building infrastructure. These characteristics align with basement environment, where mechanical equipment, structural elements, and underground location would create both isolation from some external disturbances (high frequency) while introducing specific mechanical vibrations.

Question 7: Location A- Likely Location: 3rd floor of wooden house This location has the following features: Z-axis gyro has significantly higher RRW ($4.72\text{e-}5$) and bias stability ($9.45\text{e-}5$). Wooden structures have lower mass and greater flexibility, causing more vibration transmission, especially along vertical axis, and this might be the noise source. Wind effects and structural flexing likely contribute to higher Z-axis instability.

Location B- Likely Location: ISEC basement This location has following Features: high X-axis accelerometer RRW ($9.62\text{e-}2$), high Y-axis bias stability ($1.22\text{e-}2$). Building basements typically house mechanical equipment (HVAC, pumps, generators, elevators) that produce specific vibrational frequencies. The directional nature of the disturbances suggests specific machinery or structural elements affecting particular axes. So based on this suggestions, this location likely would be the ISEC basement.

Location C- Likely Location: 5th floor of ISEC. The analysis has the following features: Very high X-axis gyro bias stability ($2.13\text{e-}4$). The source of the noise is likely due to upper floors experience building sway, wind effects, and vibrations from roof equipment. The irregular readings suggest influence from building structural dynamics at height.

Lastly, **Location D** will likely be Snell library basement. The analysis shows this location has very low gyro noise parameters across all axes, better overall bias stability. This might be due to the fact that libraries require quiet environments; basements offer thermal stability, isolation from external vibrations, and controlled environments.

Question 8: Based on the analysis across all locations, optimal Allan variance measurement conditions require an underground or basement environment with effective isolation from mechanical equipment, preferably within massive concrete structures that naturally dampen vibrations. The ideal testing space should be at a significant distance from vibration sources such as elevators, HVAC systems, and pedestrian traffic.

Question 9: To characterize a new sensor with unknown performance, I would implement a testing approach beginning with controlled laboratory measurements to establish baseline performance. First, I would conduct tests in an isolated environment to determine the sensor's noise characteristics. Then, I would progressively introduce the sensor to various realistic environments resembling its intended operating conditions, including different vibration profiles, temperature ranges, and electromagnetic conditions. By collecting long-duration stationary data in each environment and performing Allan variance analysis, I could identify specific noise sources and their magnitudes.

4 Conclusion

In this lab, we collected both stationary and dynamic motion data to analyze sensor performance. We extracted and plotted time series data from the gyroscope, accelerometer, and magnetometer in stationary conditions, and analyzed the correlation between IMU readings and physical motion in dynamic tests. Also, performance parameters including angle random walk, bias stability, and rate random walk were analyzed using Allan variance analysis on long-term datasets from different locations.